

# The role of ionization in the shock acceleration theory

Giovanni Morlino<sup>1\*</sup>

<sup>1</sup>*INAF-Osservatorio Astrofisico di Arcetri, Largo E. Fermi, 5, 50125 Firenze, Italy*

Accepted —. Received —

## ABSTRACT

We study the acceleration of heavy nuclei at SNR shocks taking into account the process of ionization. In the interstellar medium atoms heavier than hydrogen which start the diffusive shock acceleration (DSA) are never fully ionized at the moment of injection. We will show that electrons in the atomic shells are stripped during the acceleration process, when the atoms already move relativistically. For typical environment around SNRs the dominant ionization process is the photo-ionization due to the background Galactic radiation. The ionization has two interesting consequences. First, because the total photo-ionization time is comparable to the beginning of the Sedov-Taylor phase, the maximum energy which ions can achieve is smaller than the standard result of the DSA, which predict  $E_{\max} \propto Z_N$ . As a consequence the structure of the CR spectrum in the *knee* region can be affected. The second consequence is that electrons are stripped from atoms when they already move relativistically hence they can start the DSA without any pre-acceleration mechanism. We use the linear quasi-stationary approach to compute the spectrum of ions and electrons accelerated after being stripped. We show that the number of these secondary electrons is enough to account for the synchrotron radiation observed from young SNRs, if the amplification of the magnetic field occurs.

**Key words:** shock acceleration – ionization – non thermal emission – supernova remnant

## 1 INTRODUCTION

The bulk of Galactic cosmic rays (CRs) is largely thought to be accelerated at the shock waves associated with supernova remnants (SNRs) through the mechanism of diffusive shock acceleration (DSA). A key feature of this mechanism is that the acceleration rate is proportional to the particle charge. This property is especially appealing if one tries to explain the structure of the knee in the CR spectrum: if we assume that the maximum energy of accelerated particles scales with the charge of the particles involved, a knee arises naturally as a superposition of spectra of chemicals with different nuclear charges  $Z_N e$  (Hörandel 2003). This result is based on the assumption that nuclei are completely ionized during the acceleration. On the other hand when ions are injected into the acceleration process they are unlikely to be fully stripped, especially if of high nuclear charge.

The atoms relevant for the injection are those present in the circumstellar medium where the forward shock propagates. The temperature of this plasma varies from  $10^4$  K if the SNR expands into the regular ISM, up to  $10^6$  K if the expansion occurs into the bubble created by the progenitor's wind. If  $T \sim 10^4$  K even hydrogen is not fully ion-

ized, as demonstrated by the presence of Balmer lines associated with shocks in some young SNRs (Chevalier et al. 1980; Sollerman et al. 2003; Heng 2009). For  $T \sim 10^6$  only atoms up to  $Z_N = 5$  can be completely ionized (Porquet et al. 2001).

The typical assumption made in the literature is that atoms lose all electrons in the atomic orbitals soon after the beginning of the acceleration process, namely that the ionization time needed to strip all the electrons is much smaller than the acceleration time. In spite of this assumption in Morlino (2009) we showed that, for a typical SNR shock, the ionization time is comparable with the acceleration time, hence electrons are stripped when ions already move relativistically. This fact has two important consequences: 1) the maximum energy of ions can be reduced with respect to the standard prediction of DSA and 2) the ejected electrons can easily start the acceleration process because they already move relativistically.

The possibility that ionization can provide a source of relativistic electrons is especially relevant because the question of how electrons are injected into the DSA is still an unsolved issue. DSA applies only for particles with a Larmor radius larger than the typical shock thickness, which is of the order of Larmor radius of the shocked downstream thermal ions. The injection condition can be easily fulfilled

\* E-mail: morlino@arcetri.astro.it

for supra-thermal protons which reside in the highest energy tail of the Maxwellian distribution. The injection of heavier ions is, in principle, even easier than that of protons in that their Larmor radius is larger assuming they have the same proton temperature (which could be not the case). On the other hand the same argument tells that electrons cannot be injected from the thermal bath because, even if we assume equilibration between electrons and protons, the Larmor radius of electrons is a factor  $(m_e/m_p)^{1/2}$  smaller than that of protons. Only electrons which are already relativistic can cross the shock and start the DSA.

Most proposed solutions to the electron injection problem involve some kind of pre acceleration mechanism driven by plasma instabilities able to accelerate thermal electrons up to mildly relativistic energy. For instance Galeev (1984) showed that magnetosonic turbulence excited by a beam of reflected ions ahead of the shock can accelerate electrons along the magnetic field lines thanks to their Cerenkov interaction with excited waves. Other studies predict that electrons can be effectively preaccelerated by self-generated whistler waves (Levinson 1992, 1996). More recently Amano & Hoshino (2009) showed that efficient electron acceleration can happen in perpendicular shocks due to “shock surfing” of electrons on electrostatic waves excited by Buneman instability at the leading edge of the shock foot. A different mechanism proposed by Riquelme & Spitkovsky (2010), can take place in quasi-perpendicular shocks and is driven by the presence of oblique whistler waves excited by the returning ions in the shock foot. The study of these electromagnetic pre-acceleration mechanisms can be only performed using numerical techniques which showed that the fraction of injected electrons strongly depend on the values of initial conditions (like magnetic field strength and orientation) and are difficult to apply to realistic cases.

In this paper we investigate in detail the process of ionization applied to the acceleration of heavy ions, presenting the full steady-state solution for shock acceleration in the test particle approach.

The paper is organized as follows: in §2 we compare the acceleration time of ions with the ionization time due both to photo-ionization and to Coulomb scattering showing that the former dominates on the latter. In §3 we use the linear acceleration theory to compute the maximum energy achieved by different chemical specie when the ionization process is taken into account. In §4 we compute the distribution function of both ions and electrons in the framework of linear acceleration theory including the term due to ionization. We conclude in §5.

## 2 IONIZATION VS. ACCELERATION TIME

In this section we show that the ionization of different chemical species occurs during the acceleration process on a timescale which is comparable with the acceleration time needed to achieve relativistic energies. We also show that the ionization due to Coulomb collision is generally negligible compared with the photo-ionization due to the interstellar radiation field (ISRF).

Let us consider atoms of a single chemical specie  $N$  with nuclear charge  $Z_N$  and mass  $m_N = Am_p$ , which start the DSA with initial charge  $Z < Z_N$  and momentum  $p_{inj}$ . We

want to compute which is the ionization time needed to lose one electron, changing the net charge from  $Z$  to  $Z + 1$  and which is the momentum  $p$  that ions reach when ionization occurs.

For simplicity we compute the acceleration time in the framework of linear shock acceleration theory for plane shock geometry: i.e. we assume that during the ionization time needed to strip one single electron, the shock structure does not change. If a particle with momentum  $p$  diffuses with a diffusion coefficient  $D(p)$ , the well know expression for the acceleration time is:

$$\tau_{acc}(p_{inj}, p) = \int_{p_{inj}}^p \frac{3}{u_1 - u_2} \left( \frac{D_1(p)}{u_1} + \frac{D_2(p)}{u_2} \right) \frac{dp}{p}, \quad (1)$$

where  $u$  is the plasma speed in the shock rest frame, and the subscript 1 (2) refers to the upstream (downstream) quantities (note that  $u_{shock} \equiv u_1$ ). The downstream plasma speed is related to the upstream one through the compression factor  $r$ , i.e.  $u_2 = u_1/r$ . We limit our considerations to strong shocks, which have compression factor  $r = 4$ , and we assume Bohm diffusion coefficient, i.e.  $D_B = r_L \beta c / 3$ , where  $\beta c$  is the particle speed and  $r_L = pc / ZeB$  is the Larmor radius. The turbulent magnetic field responsible for the particle diffusion is assumed to be compressed downstream according to  $B_2 = r B_1$ . Even if this relation applies only for the magnetic component parallel to the shock plane, such assumption does not affect strongly our results. It is useful to define the instantaneous acceleration time as  $t_{acc} \equiv d\tau / (dp/p)$ . Using all previous assumptions  $t_{acc}$  can be expressed as follows:

$$t_{acc}(p) = 0.85 \frac{\beta p}{m_N c} B_{\mu G}^{-1} u_8^{-2} \left( \frac{A}{Z} \right) \text{ yr}. \quad (2)$$

Here the upstream magnetic field is expressed in  $\mu G$  and the shock speed is  $u_1 = u_8 10^8 \text{ cm/s}$ . Notice that, when  $B$  and  $u$  are assumed constant,  $\tau_{acc}$  reduces to  $t_{acc}$  for  $p_{inj} \ll p$  and  $D \propto p$ . To compute the energy reached by particles when the ionization event occurs, Eq. (2) has to be compared with the ionization time scale. Ionization can occur either via Coulomb collisions with thermal particles or via photo-ionization with background photons. Whether the former process dominates on the latter depends on the ISM number density compared to the ionizing photon density. In the following we show that photo-ionization dominates when SNRs are young and expand in a typical ISM.

As soon as the ions start the DSA, the photo-ionization can occur only when the energy of background photons,  $\epsilon'$ , as seen in the ion rest frame, is larger than the ionization energy  $I$ . Atoms moving relativistically with a Lorentz factor  $\gamma$  see a distribution of photons peaked in the forward direction of motion, with a mean photon energy  $\epsilon' = \gamma\epsilon$ . The photo-ionization cross section can be estimated using the simplest approximation for the  $K$ -shell cross section of hydrogen-like atoms with effective nuclear charge  $Z$ , i.e. (Heitler 1954):

$$\sigma_{ph}(\epsilon') = 64 \alpha^{-3} \sigma_T Z^{-2} (I_{N,Z} / \epsilon')^{7/2} \quad (3)$$

where  $\sigma_T$  is the Thompson cross section and  $\alpha$  is the fine structure constant and  $I_{N,Z}$  is the ionization energy threshold for the ground state of the chemical specie  $N$  with  $Z_N - Z$  electrons. The numerical values of  $I_{N,Z}$  can be found in the literature (see e.g. Allen (1973) for elements up to  $Z_N = 30$ ). To get the full photo-ionization time we need to integrate over the total photon energy spectrum, i.e.:

$$\tau_{\text{ph}}^{-1}(\gamma) = \int d\epsilon \frac{dn_{\text{ph}}(\epsilon)}{d\epsilon} c \sigma_{\text{ph}}(\gamma\epsilon), \quad (4)$$

where  $dn_{\text{ph}}/d\epsilon$  is the photon spectrum as seen in the plasma rest frame. Because the photo-ionization cross section decreases rapidly with increasing photon energy, for a fixed ion speed the relevant ionizing photons are only those with energy close to the threshold, i.e.  $\epsilon \simeq I_{N,Z}/\gamma$ , measured in the plasma frame. The corresponding numerical value is:

$$\tau_{\text{ph}}(\gamma) \simeq 0.01 Z^2 (n_{\text{ph}}(I_{N,Z}/\gamma)/\text{cm}^{-3})^{-1} \text{ yr}. \quad (5)$$

We assume that the maximum possible acceleration time is equal to the Sedov-Taylor time,  $t_{ST}$ , corresponding to the end of the free expansion phase. Comparing  $t_{ST}$  with Eq. (5), we see that the photons which can be relevant for ionization are only those with a number density  $n_{\text{ph}} > 10^{-5} Z^2 (t_{ST}/10^3 \text{ yr})^{-1} \text{ cm}^{-3}$ . For this reason we can neglect the high energy radiation coming from the remnant itself because the typical number density of the x-ray photons is less than  $10^{-7} \text{ ph/cm}^{-3}$ .

An important consequence of the photo-ionization is that electrons are stripped from the atoms with a kinetic energy  $\ll m_e c^2$  as measured in the atom rest frame. Hence, if the parent atoms move relativistically in the plasma rest frame, electrons move with the same Lorentz factor and the same direction of the parent atoms. This property will be used in §4 to simplify the calculation of electrons spectrum.

Now we consider the ionization of accelerated ions due to Coulomb collisions with protons and electrons of the thermal plasma. We neglect the thermal energy of those particles and we consider the process in the ion's rest frame. The role of collisions is mainly relevant during the very initial stage of acceleration, namely when the kinetic energy of incident particle,  $E_{\text{kin}}$ , is close to the ionization energy,  $I$ , as seen in the ion's rest frame. This is a consequence of the shape of ionization cross section which has a peak value for  $E_{\text{kin}} \sim I$  and rapidly decreases for larger energies. A good upper limit for the peak value of the cross section is provided by the classical (non relativistic) Thomson approach (Allen 1973), which gives a maximum for  $E_{\text{kin}} = 2I$  equal to:

$$\sigma_{\text{coll}}^{\text{max}} = \pi a_0^2 N_e I_{\text{Ryd}}^{-2}. \quad (6)$$

where  $a_0$  is the Bohr radius,  $I_{\text{Ryd}}$  is the ionization energy expressed in Rydberg unity and  $N_e$  is the number of electrons in the atomic orbital considered. For larger energies the Thomson cross section decreases like  $E_{\text{kin}}^{-2}$  while the asymptotic behavior predicted by the quantum mechanics is  $\sigma \sim \log(E_{\text{kin}})/E_{\text{kin}}$ . This implies that the collisional ionization time has a minimum for  $\sigma = \sigma_{\text{coll}}^{\text{max}}$  and than increases. In order to get this minimum value one must average the contribution of collisions in the upstream and downstream region. Assuming equal density for thermal protons and electrons  $n_e = n_p \equiv n_1$ , the result is (Morlino 2009):

$$\tau_{\text{coll}}^{\text{min}} \approx [c \sigma_{\text{coll}}^{\text{max}} n_1 (1+r)]^{-1} = 0.0024 I_{\text{Ryd}}^2 \left( \frac{n_1}{\text{cm}^{-3}} \right)^{-1} \text{ yr}. \quad (7)$$

Equation (7) is valid in the non relativistic regime. In this regime the acceleration time increases only like  $t_{\text{acc}} \sim p \sim E_{\text{kin}}^{1/2}$ . As a consequence the collisional ionization can occur only if the acceleration time needed to have  $E_{\text{kin}} = 2I$  is larger than  $\tau_{\text{coll}}^{\text{min}}$ . Let us call  $\gamma^*$  the Lorentz factor which corresponds to this condition, namely  $\gamma^* = 1 + 2I/m_e c^2$ .

Comparing Eq. (7) with Eq. (2), the condition  $t_{\text{acc}}(\gamma^*) = \tau_{\text{coll}}^{\text{min}}$  provides a lower limit for the upstream density, i.e.:

$$n_{1,\text{min}} = 27 I_{\text{Ryd}} B_{\mu\text{G}} u_8^2 (Z/Z_N) \text{ cm}^{-3}. \quad (8)$$

Hence for  $n_1 < n_{1,\text{min}}$  ions are accelerated up to relativistic energies before being ionized by collisions. Notice that we neglected collisions with atoms heavier than hydrogen: such contribution could reduce the ionization time by less than a factor 2, hence our main conclusions remain valid.

Now, in order to understand the relevance of collisions in the relativistic regime we can use the asymptotic Bethe cross section valid in the limit  $E_{\text{kin}} \gg m_e c^2$ , (Bethe 1930). The relativistic formulation of this cross section for the total ionization is often written as (Kim et al. 2000):

$$\sigma_{\text{RBethe}}(\gamma) = \frac{4\pi a_0^2 \alpha^2}{\beta^2} [M^2 (\ln(\gamma^2 \beta^2) - \beta^2) + C_R]. \quad (9)$$

The two constant  $M^2$  and  $C_R$  are related to the atomic form factors of the target and are independent of the incident particle energy. Their exact numerical values are very difficult to compute with some noticeable exception like H-like atoms. In principle they can also be inferred from photo-ionization experiments but in practice they are known only for a bunch of targets. Nevertheless from theory we know that  $M^2 \sim N_e/I_{\text{Ryd}}$ , while  $C_R \sim 10M^2$  (Inokuti 1971; Kim et al. 2000). Using these estimates in the ultra relativistic limit we have  $\sigma_{\text{RBethe}}/\sigma_{\text{coll}}^{\text{max}} \lesssim 10^{-3}$ . This result implies that Coulomb collisions are much less important in the relativistic regime with respect to the non relativistic one.

In order to compare the photo-ionization with the collisional ionization times, in Fig. 1 they have been plotted together with the acceleration time for three different H-like ions:  $\text{He}^+$ ,  $\text{C}^{5+}$  and  $\text{Fe}^{25+}$ . The characteristic time are plotted as functions of the ion's Lorentz factor. The acceleration time  $t_{\text{acc}}$ , plotted with solid lines, is shown for two different choices of parameters:  $u_1 = 1000 \text{ km/s}$ ;  $B_1 = 3\mu\text{G}$  (upper line) and for  $u_1 = 10^4 \text{ km/s}$ ,  $B_1 = 20\mu\text{G}$  (lower line). The photo-ionization time  $\tau_{\text{ph}}$  (dashed lines) is computed according to Eq. (4) using the cosmic microwave background plus the Galactic ISRF as reported by Porter & Strong (2005). The ISRF strongly changes going from the center towards the periphery of the Galaxy, hence, the photo-ionization depends on the SNR location. In order to evaluate this variation we show  $\tau_{\text{ph}}$  using the ISRF in the Galactic Center (lower dashed line) and the one at 12 kpc far away from the Galactic Center in the Galactic plane (upper dashed lines). Finally with dot-dashed lines we plot the collisional ionization time for the upstream density  $n_1 = 1\text{cm}^{-3}$ : the thin horizontal line corresponds to the non relativistic lower limit expressed in Eq. (7),  $\tau_{\text{coll}}^{\text{min}}$ , while the thick line is calculated using the relativistic Bethe cross section for H-like atoms. In this case the values of the parameters used in the Bethe cross section are  $M^2 = 0.30/Z_N^4$  and  $C_R = 4.30/Z_N^4$  (Bethe 1930). Fig. 1 clearly shows that the collisional ionization can be neglected for the case of young SNRs expanding into a medium with a number density less than a few  $\text{cm}^{-3}$ . The photo-ionization is the dominant process even for SNR located far away from the Galactic Center. This consideration is strengthened in the case of core-collapse SNRs, which typically expand into the bubble created by the progenitor wind, whose density is usually assumed  $\sim 10^{-2} \text{ cm}^{-3}$ . The only phase where the collisional ionization could domi-

nate over photo-ionization is the very initial stage, when the shock is expanding into the progenitor’s wind, whose density is much higher. This phase typically lasts few years and in this work it will be neglected.

In Fig. 1 the value of  $\gamma$  where  $t_{\text{acc}}$  cross  $\tau_{\text{ph}}$ , identifies the Lorentz factor of the ejected electrons they are for. Looking at the upper plot it is clear that even electrons coming from the ionization of  $\text{He}^+$  can, in principle, start the DSA, having a typical Lorentz factor  $\gtrsim 10$ . In fact, as discussed in Morlino (2009) the minimum Lorentz factor required for electrons to be injected is  $\gamma_{\text{inj}} \sim 3 - 30$  for typical parameters of SNR shocks.

### 3 MAXIMUM ENERGY OF IONS

The process of ionization can affect the maximum energy that nuclei achieve during the acceleration, especially those with large nuclear charge. It is worth stressing that the knowledge of the maximum energy is intimately connected with two important aspects of the CR spectrum: the interpretation of the *knee* structure and the transition region from Galactic to extragalactic component. The *knee* is commonly interpreted as due to the superposition of the spectra of all chemicals with different cutoff energies. Using the flux of different components measured at low energies it has been shown that the knee structure is well reproduced if one assumes that the maximum energy of each specie  $E_{\text{max},N}$  is proportional to the nuclear charge  $Z_N$  (Hörandel 2003). Nevertheless the superposition of subsequent cutoff seems to be confirmed by the measurements of the spectrum of single components in the knee region: data presented by the KASCADE experiments show that the maximum energy of He is  $\sim 2$  times larger than that of the protons (Antoni et al. 2005). From the theoretical point of view the relation  $E_{\text{max},N} \propto Z_N$  is clearly predicted by DSA if one assume that the diffusion coefficient is rigidity-dependent. On the other hand this is correct only provided that during the acceleration process nuclei are completely ionized otherwise the maximum energy is proportional to the effective charge of the ions rather than to their nuclear charge.

Now, the maximum energy is thought to be achieved at the beginning of the Sedov-Taylor phase ( $t_{ST}$ ) (Blasi, Amato & Caprioli 2007). For later times,  $t > t_{ST}$ , the shock speed decreases faster than the diffusion velocity, hence particles at the maximum energy can escape from the accelerator and the maximum energy cannot increase further. It is worth noting that the process of escaping is not completely understood in that it strongly depends on the turbulence produced by the same escaping particles and on the damping mechanisms of the turbulence itself (Caprioli et al. 2010). Anyway here we assume that the maximum energy,  $E_{\text{max}}$ , is achieved at  $t = t_{ST}$ . If the total ionization time is comparable, or even larger than  $t_{ST}$ , we do expect that  $E_{\text{max}} < E_{\text{max}}^0$ , where we call  $E_{\text{max}}^0$  the maximum energy achieved by ions which are completely ionized since the beginning of acceleration.

A consistent treatment of the ionization effects would require the use of time-dependent calculation. However our aim is to get a first order approximation of the effect of ionization. This can be achieved using the quasi-stationary version of the linear acceleration theory.

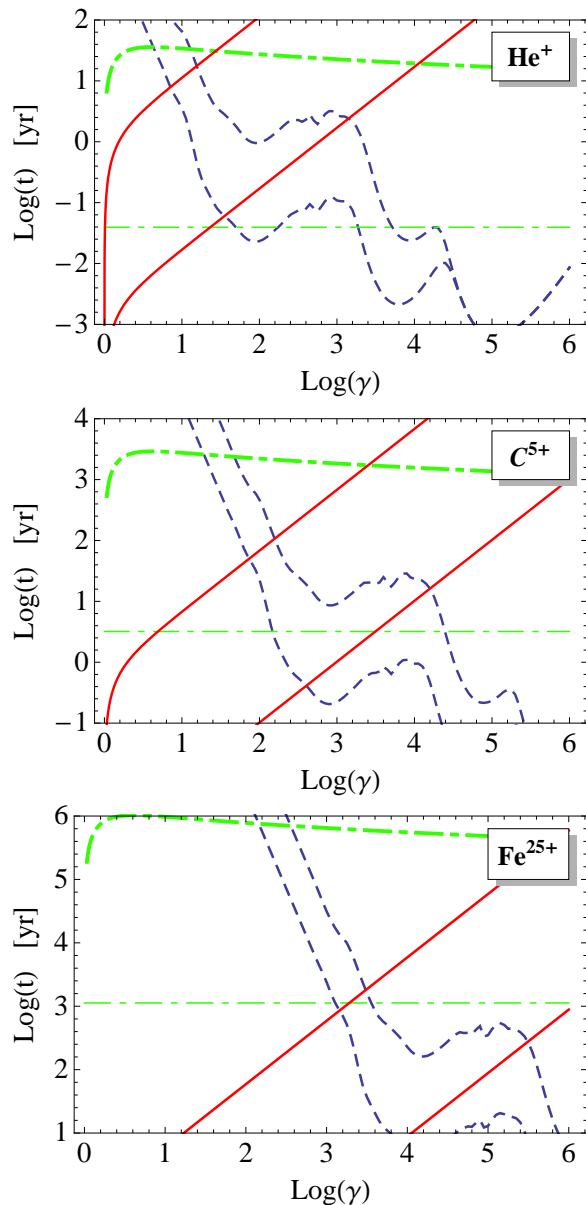


**Figure 1.** Comparison between acceleration time (solid lines), photo-ionization time (dashed) and collisional ionization time (dot-dashed) for three hydrogen-like ions:  $\text{He}^+$ ,  $\text{C}^{5+}$  and  $\text{Fe}^{25+}$  (from top to bottom). Acceleration and photo-ionization times are shown with two curves representing two different set of parameters, as explained in the text. The horizontal thin dot-dashed line represent the lower limit for the collisional ionization time, Eq. (6), while the thick dot-dashed line is computed using the Bethe cross section with a plasma density  $n_1 = 1\text{cm}^{-3}$ .

In order to compute  $E_{\text{max}}$  the first piece of information we need is the initial ionization level of ions. In the case of volatile elements, which exist mainly in the gas-phase, the level of ionization is easy to estimate being only a function of the plasma temperature: ions are ionized up to a level such that the ionization energy is of the same order of the kinetic energy of thermal electrons as seen in the ion’s rest frame. On the other hand refractory elements are largely locked into solid dust grains. This occurs both in

the regular ISM as well as in stellar winds. As claimed by Ellison, Drury & Meyer (1997) there are evidences that elements condensed in dust grains are efficiently injected into the DSA thanks to the fact that dust grains can be easily accelerated up to energies where the grains start to be sputtered. A non negligible fraction of the atoms expelled by sputtering are energetic enough to start the DSA. In this scenario the ionization level of ejected atoms is very difficult to predict in that depends on the structure of the grains. However a reasonable assumption could be that ions preserve all the electrons in the inner shells which are not shared in the orbitals of the crystal structure of the grains. Moreover, as noted by Ellison, Drury & Meyer (1997), if the ejected ion is highly ionized its electron affinity is strong and electron-exchange with the atoms of thermal plasma could reduce the level of ionization up to the equilibrium one. For these reasons, in the following calculation, we neglect the complication arising from the dust sputtering process and we assume that the level of ionization is only determined by the plasma temperature.

Let us consider a single ion injected with momentum  $p_0$  and total charge  $Z_1$ . The ion undergoes acceleration at a constant rate  $\propto Z_1$  during a time equal to the ionization time needed to lose one electron,  $\tau_{\text{ph},1}$ , when it achieves the momentum  $p_1$ . Notice that we include only the photo-ionization because, as we saw in the previous paragraph, for typical density of the external medium around the SNR ( $n_0 \lesssim 1 \text{ cm}^{-3}$ ), the Coulomb collisions can be neglected. In order to compute simultaneously  $\tau_{\text{ph},1}$  and  $p_1$  we have to equate the acceleration time with the ionization time:

$$\tau_{\text{ph},1}(p_1/m_N c) = \tau_{\text{acc}}(p_0, p_1) = t_{\text{acc}}(p_1) - t_{\text{acc}}(p_0). \quad (10)$$

The last equality holds because we use Bohm diffusion and because we assume that the shock velocity and the magnetic field both remain constant during  $\tau_{\text{ph},1}$ . Moreover we saw that the photo-ionization occurs when ions already move relativistically, hence using Eq. (2) we set  $\beta = 1$ . Eq. (10) gives

$$\frac{p_1}{m_p c} = \frac{p_0}{m_p c} + \frac{Z_1 B_1 u^2}{1.7 Z_N} \tau_{\text{ph},1} (p_1/m_N c), \quad (11)$$

where the subscript 1 label the quantities during the time  $\tau_{\text{ph},1}$ . In Eq. (11)  $B$  and  $u$  are expressed in units of  $\mu G$  and  $u_8$  while  $\tau_{\text{ph},1}$  is expressed in yr. Once the background photon distribution is known Eq. (11) can be solved numerically in order to get  $p_1$  and  $\tau_{\text{ph},1}$ . After the first ionization the acceleration proceeds at a rate proportional to  $Z_2 \equiv Z_1 + 1$  during a time  $\tau_{\text{ph},2}$ , which is the time needed to lose the second electron. Applying Eq. (11) repeatedly for all subsequent ionization steps, we get the momentum when the ionization is complete. If the total ionization time,  $\tau_{\text{ion}}^{\text{tot}}$ , is smaller than the Sedov time, in order to get the maximum momentum we need to add the further acceleration during the time  $(t_{ST} - \tau_{\text{ion}}^{\text{tot}})$ . The final expression for the maximum momentum can be written as follows:

$$\frac{p_{\text{max}}}{m_p c} = \sum_{k=1}^{Z_N - Z_0} \frac{Z_k B_k u_k^2 \tau_{\text{ph},k}}{1.7 Z_N} + \theta (t_{ST} - \tau_{\text{ion}}^{\text{tot}}) \sum_{i=1}^M \frac{B_i u_i^2}{1.7 M}, \quad (12)$$

where we neglected the contribution of  $p_0$ . The last term has been written as a sum over  $M$  time-steps in order to handle the case where magnetic field and shock speed change with time.

Now we can quantify the effect of ionization in the determination of  $p_{\text{max}}$ . The simplest approximation we can do is to assume  $u_{sh}$  and  $B$  constant during the free expansion phase, i.e. up to  $t = t_{ST}$ . In order to estimate  $t_{ST}$  we consider two different situations which can represent a typical type I/a and a core-collapse supernovae. In the first case the supernova explodes in the regular ISM with typical density and temperature  $n_1 = 1 \text{ cm}^{-3}$  and  $T_0 = 10^4 \text{ K}$ . On the other hand SNRs generated by very massive stars expand into medium with higher temperature. This could be either the bubble generated by the progenitor's wind or a so called *super-bubble*, a region where an elevate rate of SN explosions produces a diluted and hot gas (Higdon & Lingenfelter 2005). In both cases typical values for the density and temperature inside the bubble are  $n_1 = 10^{-2} \text{ cm}^{-3}$  and  $T_0 = 10^6 \text{ K}$ . For both type I/a and core-collapse supernovae we assume the same value for the explosion energy  $E_{SN} = 10^{51} \text{ erg}$ , and mass ejecta  $M_{ej} = 1.4 M_{\odot}$ . The resulting Sedov time is  $t_{ST} = 470 \text{ yr}$  and  $t_{ST} = 2185 \text{ yr}$ , respectively. The average shock speed during the free expansion phase is  $u_{sh} \simeq 6000 \text{ km/s}$  in both cases.

It is worth stressing that if one would consider a more realistic scenario for core-collapse SNe it is important to take into account the type of the progenitor and its wind, in order to provide a better estimate of the ejected mass and of the bubble's dimension and density. These parameters strongly affect the value of  $t_{ST}$ , which determines how effective is the ionization in reducing the maximum energy: indeed for  $t_{ST} \gg 10^3 \text{ yr}$  the role of ionization becomes negligible, as we see below.

The last parameter we need is the magnetic field strength. We stress that our aim is only to estimate the effect of ionization in the scenario where the SNRs indeed produce the observed CRs spectrum and the *knee* is interpreted as the superposition of a rigidity-dependent cutoff of different species. For this reason we assume that both scenarios are able to accelerate protons up to the *knee* energy, i.e.  $E_{\text{knee}} = 3 \cdot 10^{15} \text{ eV}$ . This condition gives  $B_1 = 160 \mu G$  and  $35 \mu G$  for type I/a and core-collapse cases, respectively. We note that the chosen values of magnetic field strength are consistent with those predicted by the CR-induced magnetic field amplification.

In Fig. (2) we plot the maximum energy achieved at the beginning of the Sedov-Taylor phase by different chemical species, from H up to Zn ( $Z_N = 30$ ). The two panels show the case of type I/a (upper) and core-collapse SNR (lower) previously described. Each panel contains four lines: thin solid lines are the maximum energy achieved by ions which start the acceleration completely stripped,  $E_{\text{max}}^0$ , while the remaining lines show  $E_{\text{max}}$  computed according to Eq. (12) for three different locations of the SNR in the Galactic plane: at the center of the Galaxy and at 4 and 12 kpc away from the Galactic Center. Looking at the upper panel we see that the maximum energy achieved by different nuclei in type I/a SNRs does not increase linearly with  $Z_N$ , instead it reaches a plateau for  $Z_N \gtrsim 25$  at a distance  $d = 4 \text{ kpc}$  and for  $Z_N \gtrsim 15$  at  $d = 12 \text{ kpc}$ . Only for SNRs located in the Galactic bulge the reduction of the maximum energy is negligible, at least for elements up to  $Z_N = 30$ . The effect of ionization is much less relevant for core collapse SNRs: only those remnants located at a distance of 12 kpc show a noticeable reduction of  $E_{\text{max}}$ .

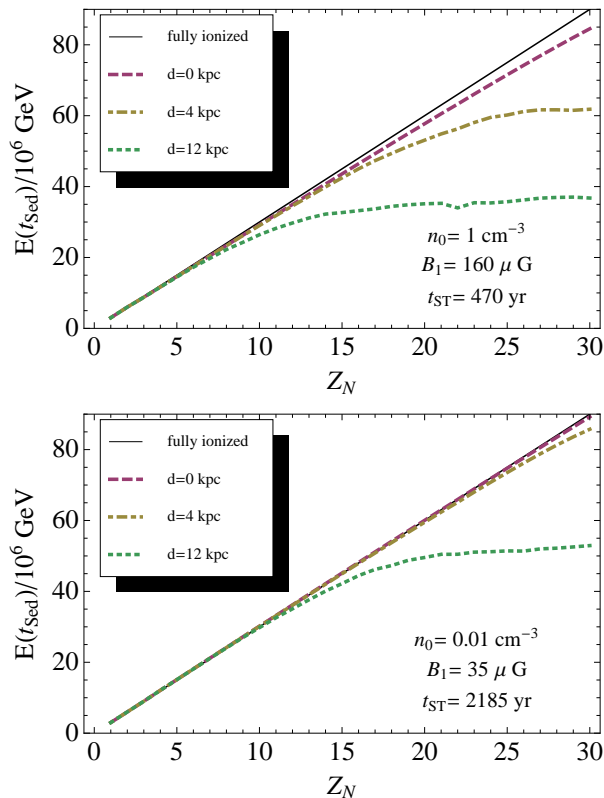


**Figure 2.** Maximum energy achieved by chemical specie with nuclear charge  $Z_N$  (ranging from H to Zn) at the beginning of the Sedov phase. The upper panel shows the case of type I/a SNR, expanding into a medium with density  $\rho_0 = 1 \text{ cm}^{-3}$  while the lower panel is for core-collapse SNR expanding into a diluted bubble ( $\rho_0 = 0.01 \text{ cm}^{-3}$ ). The thin solid line shows the maximum energy achieved by atoms which are fully ionized since the beginning of the acceleration, while the other curves are computed including the photo-ionization due to ISRF for SNR located at three different distance  $d$  from the Galactic Center, as specified in the caption.

	$t_{ST}(\text{yr})$	$d$ (kpc)	$\tau_{\text{ion}}^{\text{tot}}(\text{yr})$	$E_{\text{max}}/E_{\text{max}}^0$
type I/a	470	0	76 (137)	0.98 (0.52)
	"	4	356 (385)	0.80 (0.39)
	"	12	1446 (2932)	0.48 (0.24)
core-collapsed	2185	0	113 (142)	0.99 (0.58)
	"	4	264 (374)	0.97 (0.48)
	"	12	2860 (2780)	0.65 (0.35)

**Table 1.** Total photo-ionization time and normalized maximum energy achieved by iron nuclei for the two idealized cases of type I/a and core-collapsed SNRs, which are located at a distance  $d = 0, 4$  and  $12$  kpc from the Galactic Center. For comparison also the Sedov time is listed. The bare numbers represent the case where the shock speed and the magnetic field are both constant during the free expansion phase (as in Fig. 2), while the numbers in round brackets are computed assuming  $u_{sh}$  and  $B_1$  which evolve in time according to the model explained in the text (see also Fig. 3).

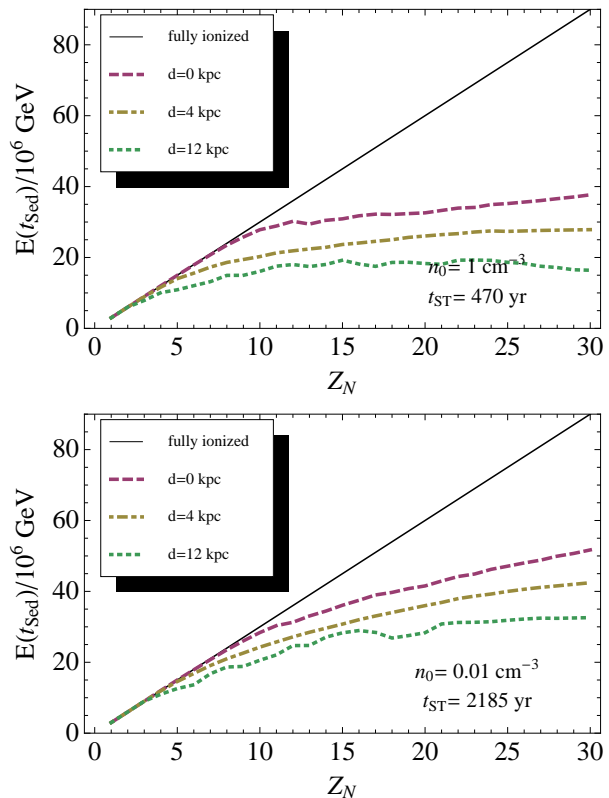


**Figure 3.** The same as in Fig. 2 but for a scenario where both the shock speed and the magnetic field strength evolve with time, as explained in the text.

The numerical results for iron nuclei corresponding to all cases shown in Fig. 2 are summarized in Table 1. Here we report the total ionization time and the ratio between the energy achieved at  $t_{ST}$  and the maximum theoretical energy achieved by bare nuclei,  $E_{\text{max}}^0$  (notice that the numbers in brackets refer to Fig. 3 as explained below).

The results presented in Fig. 2 are inferred using a simple steady state approach. This approach could be too reductive and one can guess how the effect due to the ionization process changes when the full evolution history of the remnant is taken into account. Needless to say a correct calculation of the maximum energy requires not only the treatment of the evolution of the remnant but also the inclusion of nonlinear effects which consistently describe the magnetic field amplification and the back reaction of CRs onto the shock dynamics. A fully consistent treatment of the problem is beyond the purpose of this work. However we would understand whether the evolution and the nonlinearity can reduce or exacerbate the effect induced by ionization. In order to reach this goal we approximate the continuum evolution into time steps equal to the ionization times,  $\tau_{\text{ph},k}$  and we assume that the stationary approximation is valid for each time step. Under this approximation Eq. (12) can be used to include the effect of evolution if we make reasonable assumptions on how the shock speed and the magnetic field change with time. We follow Truelove & McKee (1999) for the description of the time evolution of the remnant. Specifically we adopt the solution for a remnant characterized by

a power-law profile of the ejecta (in the velocity domain) with index  $n = 7$ , expanding into an homogeneous medium. For this specific case Truelove & McKee (1999) provide the following expression for the velocity of the forward shock (see their Table 7):

$$u_1(t)/u_{ch} = 0.606 (t/t_{ch})^{-3/7} \quad (\text{for } t < t_{ST}) \quad (13)$$

where  $u_{ch} = (E_{SN}/M_{ej})^{1/2}$ ,  $t_{ch} = E_{SN}^{-1/2} M_{ej}^{5/6} \rho_1^{-1/3}$  and  $t_{ST} = 0.732 t_{ch}$ . We adopt the same values of  $E_{SN}$ ,  $M_{ej}$  and  $\rho_1$  used in the two cases above.

For what concern the magnetic field we assume that the amplification mechanism is at work, converting a fraction of the incoming kinetic energy flux into magnetic energy density downstream of the shock. The simplest way to write this relation is:

$$B_2^2(t)/(8\pi) = \alpha_B \rho_1 u_1^2(t). \quad (14)$$

We always assume  $B_2 = 4B_1$ . The parameter  $\alpha_B$  hides all the complex physics of magnetic amplification and particle acceleration. For the sake of completeness we mention here that in the case of resonant streaming instability  $\alpha_B \propto \xi_{cr} v_A/u_1$ , where  $\xi_{cr}$  is the efficiency in CRs and  $v_A$  is the Alfvén velocity, while in the case of resonant amplification  $\alpha_B \propto \xi_{cr} u_1/4c$  (Bell 2004). However such relations cannot be applied in a straightforward way since they require using a non linear theory. Here we prefer to make the simplest assumption, taking  $\alpha_B$  as a constant. We determine its value from the same condition previously used to fix the value of the constant magnetic field: namely we assume that for  $t = t_{ST}$  the energy of protons is  $3 \cdot 10^{15}$  eV. This condition gives  $\alpha_B = 3.25 \cdot 10^{-3}$  and  $6.80 \cdot 10^{-3}$  for type I/a and core-collapse cases, respectively. It is worth noting that in the case of some young SNRs the value of  $\alpha_B$  has been estimated from the measurement of both the shock speed and the magnetic field strength. However we stress that the magnetic field cannot be determined in a completely model independent way. A possible method requires the measurement of the spatial thickness of the x-ray filaments: assuming that this thickness is determined by the rapid synchrotron losses of radiating electrons we can get the average magnetic field (see Table 2 and the listed references and also Table 1 from Caprioli et al. (2009)). Noticeably the values estimated for  $\alpha_B$  are only a factor 5–10 larger then the values we use here.

Now Eq. (12) can be used to compute the maximum momentum at  $t = t_{ST}$ . For each time-step,  $\tau_{ph,k}$ , the values of  $u_k$  and  $B_k$  are computed according to Eqs. (13) and (14), respectively, evaluated at the beginning of the time-step. In Fig. 3 we report the results for the maximum energy for the case of type I/a (upper panel) and core-collapse SNRs (lower panel). The lines have the same meanings as in Fig 2. As it is clear from both the panels, the reduction of the maximum energy is now more pronounced with respect to the stationary case shown in Fig 2. Even in the scenario of a core-collapse SNR located in the Galactic bulge, iron nuclei are accelerate only up to about one half of the maximum theoretical energy. The numerical values of  $\tau_{ion}^{tot}$  and  $E_{max}/E_{max}^0$  for iron are reported in Table 1 in round brackets. One can see that even in the cases where  $\tau_{ion}^{tot}$  does not change with respect to the stationary case, the maximum energy results smaller.

The reason why ionization is less effective when the evo-

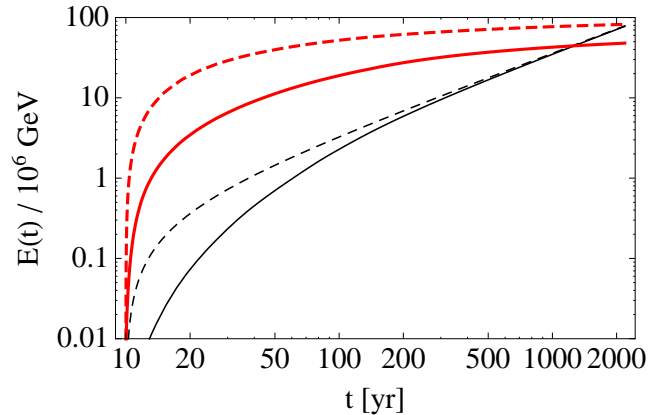


**Figure 4.** Behavior of maximum energy of Fe ions as a function of the time in the case of core-collapse SNR located in the Galactic bulge. Two different scenarios are shown: (*thin lines*) acceleration at a constant rate ( $B_1 = \text{const}$  and  $u_1 = \text{const}$ ); (*thick lines*) acceleration including the time evolution of the remnant ( $B_1 = B_1(t)$  and  $u_1 = u_1(t)$ ). The dashed lines represent the case of completely ionized ions, while the solid lines include the effect of photo-ionization.

lution is taken into account is a consequence of the fact that acceleration occurs mainly during the first stage of the SNR expansion. In fact both the shock speed and the magnetic field strength are larger at smaller times. On the other hand the effective ions' charge is small during the very initial phase of the expansion, hence the acceleration rate is smaller than its maximum possible value. In order to clarify this point in Fig. 4 we compare the energy achieved by iron nuclei as a function of the time, for the case of core collapse SNR located in the Galactic bulge, with and without the evolution. The dashed lines shown the case of completely ionized nuclei, while the solid lines take into account the ionization process. When the acceleration rate is constant (thin lines) the bulk of the acceleration occurs close to  $t_{ST}$ , when the ions are almost completely ionized, hence  $E_{max}$  and  $E_{max}^0$  are practically the same. On the other hand when the evolution is taken into account (thick lines) the acceleration mainly occurs during the first 200 yr when the ionization is still not complete and for  $t = t_{ST}$  we have  $E_{max}/E_{max}^0 = 0.58$ . Besides the numerical value, this exercise shows that the inclusion of the time evolution and non linear effects can enhance the reduction of the maximum energy due to the ionization process.

Some comments are in order. The most relevant consequence of the ionization mechanism concerns the shape of the CR spectrum in the *knee* region. As we have already discussed, the relation  $E_{max,N} \propto Z_N$  is needed in order to fit the data. Even a small deviation of the cutoff energy from the direct proportionality can affect the slope. Let us assume that the measured slope,  $s = 3.1$ , indeed results from this proportionality relation. We have  $E_{max,Fe} = 26E_{max,p}$ . Now if the maximum energy of iron decreases to 80% of its maximum value, the slope changes to  $\sim 3.33$ , while for a decrease of 50% the slope becomes  $\sim 3.94$ .

According to our results we can say that in the context of the SNR paradigm, the primary sources of CRs above the *knee* energy are most probably the core-collapse SNRs with

$M_{ej} \gg 1M_{\odot}$ . Type I/a SNRs seem unable to accelerate ions up to an energy  $Z_N$  times the proton energy, due to their small Sedov-Taylor age. This consideration is strengthened by the fact that the CR flux observed at the Earth is mostly due to the SNRs located in the solar neighborhood, rather than those located in the bulge. In fact the escaping length from the Galaxy is determined by the thickness of the Galactic halo which is  $\sim 3 - 5$  kpc, while the Galactic bulge is at 8 kpc from us.

A second comment concerns the acceleration of elements beyond the iron group. Even if the contribution of such ultra-heavy elements to the CR spectrum is totally negligible at low energies, at higher energies it can hardly be measured. In principle the contribution of ultra-heavy elements could be significant in the 100 PeV regime, which is the energy region where the transition between Galactic and extragalactic CRs occurs. Indeed several authors pointed out that a new component is needed to fit this transition region, beyond the elements up to iron accelerated in “standard” SNRs (see e.g. the discussion in Caprioli et al. (2010)). As inferred by Hörandel (2003) stable elements heavier than iron can significantly contribute to the CR spectrum in the 100 PeV regime if one assume that their maximum energy scales like  $Z_N$ . This assumption is especially appealing also for a second reason: in principle it could explain the presence of the *second knee* in the CR spectrum (Hörandel 2003); in fact the ratio  $E_{2nd\,knee}/E_{knee} \simeq 90$  is very close to the nuclear charge of the last stable nucleus, uranium, which should have  $E_{max,U} = 92E_{max,p} = 414$  PeV. On the other hand the ionization mechanism discussed here provides a strong constraint on the role of ultra-heavy elements. If the acceleration of elements heavier than Fe occurs at SNRs like those considered above, it is easy to show that they cannot achieve energies much larger than the Fe itself, because the total ionization time increases rapidly with the nuclear charge. A contribution from ultra-heavy elements is maybe possible only if they are accelerated in very massive SNRs, with  $M_{ej} \gg 1M_{\odot}$ . A second possibility that would be interesting to investigate is the acceleration during the very initial stage of the remnant, when the expansion occurs into the progenitor’s wind. In this case the high density of the wind could strongly reduce the ionization time thanks to the Coulomb collisions and nuclei could be totally stripped in a short time.

#### 4 SOLUTION OF THE TRANSPORT EQUATION

In this section we present the solution of the stationary transport equation for ions and electron accelerated at shocks when the ionization process is taken into account. We first get the solution for the distribution function of ions which can be used, in turn, as the source term responsible for the injection of electrons. We will consider only the test-particle solution, neglecting all the non linear effects coming from the back reaction of the accelerated particles onto the shock dynamics.

#### 4.1 Spectrum of ions

In order to compute the distribution function of a single chemical specie we consider separately each ionization state. Let  $f_N^Z(x, p)$  be the distribution function of the specie  $N$  with effective charge  $Z$ . The equation that describe the diffusive transport of ions in one dimension, including the ionization process reads:

$$u \frac{\partial f_N^Z}{\partial x} = D(p) \frac{\partial^2 f_N^Z}{\partial x^2} + \frac{1}{3} \frac{du}{dx} p \frac{\partial f_N^Z}{\partial p} - \frac{f_N^Z}{\tau_N^Z(p)} + Q_N^Z(x, p), \quad (15)$$

where  $u(x)$  is the fluid velocity and  $D(p)$  is the diffusion coefficient, which is a function of  $Z$  and it is assumed constant in space.  $\tau_N^Z(p)$  is the ionization time for the losses of one electron, namely for the process  $N^Z \rightarrow N^{Z+1} + e^-$ . We neglect multiple ionization processes. In order to solve Eq. (15) we need to specify the injection term  $Q_N^Z(x, p)$ . We assume that ions with the lower degree of ionization,  $Z_0$ , are injected only at the shock position ( $x = 0$ ) and at a fixed momentum  $p_{inj}$ . Hence the source term for  $f_N^{Z_0}$  is:

$$Q_N^{Z_0}(x, p) = K_N^{Z_0} \delta(x) \delta(p - p_{inj}). \quad (16)$$

The normalization constant  $K_N^{Z_0}$  is determined from the total number of particles injected per unit time. For the subsequent ionization states,  $Z > Z_0$ , the injection comes from the ionization of atoms with charge equal to  $Z - 1$ , i.e.:

$$Q_N^{Z+1}(x, p) = f_N^Z(x, p) / \tau_N^Z(p). \quad (17)$$

Equation (15) can be solved separately in the upstream and downstream regions, where the term  $du/dx$  vanishes and the equation reduces to an ordinary differential equation of second order. We label the quantities in the upstream (downstream) with a subscript 1(2) and we adopt the convention  $x < (>)0$  in the upstream (downstream). We fix the boundary conditions at the shock position such that  $f(x = 0, p) \equiv f_0(p)$ , where  $f_0(p)$  has to be determined. The boundary condition at infinity is  $\partial f / \partial x = 0$  for  $x \rightarrow \pm \infty$ . For the sake of simplicity we now drop the label characterizing the ion specie, such that  $f_N^Z \equiv f$ , and we write the solution in a compact form as follows:

$$f_i(x, p) = f_0(p) e^{\mp \lambda_{i\mp} x} \pm \int_x^{\pm \infty} \frac{Q_i(x', p)}{u_i \sqrt{1 + \Delta_i}} e^{\pm \lambda_{i\pm}(x-x')} dx' \pm \int_0^x \frac{Q_i(x', p)}{u_i \sqrt{1 + \Delta_i}} e^{\mp \lambda_{i\mp}(x-x')} dx' \mp e^{-\lambda_{i\mp} x} \int_0^{\pm \infty} \frac{Q_i(x', p)}{u_i \sqrt{1 + \Delta_i}} e^{-\lambda_{i\pm} x'} dx'. \quad (18)$$

The upper and lower signs refer to the downstream ( $i = 2$ ) and upstream ( $i = 1$ ) solutions, respectively. The dimensionless function  $\Delta(p)$  is the ratio between the diffusion time and the ionization time, i.e.  $\Delta_i(p) \equiv \frac{4D_i(p)}{u_i^2 \tau(p)}$ .  $\lambda_{i+}$  and  $\lambda_{i-}$  are the inverse of the propagation lengths along the counterstreaming and the streaming directions with respect to the fluid motion, respectively, i.e.:

$$\lambda_{i\pm}^{-1}(p) = \frac{2D_i(p)}{u_i [\sqrt{1 + \Delta_i(p)} \pm 1]}. \quad (19)$$

The quantity  $\lambda$  takes into account the diffusion, the advection and the ionization processes. One can see that in the limit where the ionization is negligible, namely when

$\tau \rightarrow \infty$ , the streaming propagation length diverges, while the counter-streaming one reduces to  $D/u$ .

The three integral terms which contribute to the distribution function in Eq. (18) have a clear physical interpretation. Let us consider the solution in the upstream: in this case the first integral represents the contribution due to particles advected with the fluid from  $-\infty$ , the second accounts for the particles diffusing in the counter-streaming direction, while the last integral takes into account the flux escaping across the shock surface. For the downstream solution the meanings of the first and second integrals are reversed, while the third one keeps the same meaning. This interpretation becomes clear if one takes the limit  $\tau \rightarrow \infty$ .

From Eq. (18) we can easily recover the standard solution where the ionization is not taken into account, assuming that the injection occurs only at the shock position and using  $\Delta_i = 0$ : in this case the integral terms vanish, and we find  $f_1(x, p) = f_0(p) \exp[-u_1 x/D_1]$  and  $f_2(x, p) = f_0(p)$ .

In order to get the complete solution we need to compute the boundary distribution function at the shock position,  $f_0(p)$ . We follow a standard technique which consists in integrating Eq. (15) around the shock discontinuity (Blasi 2002). We got the following differential equation for  $f_0(p)$ :

$$\frac{u_1 - u_2}{3} p \frac{\partial f_0}{\partial p} = \left( D_2 \frac{\partial f_2}{\partial x} \right)_{0^+} + \left( D_1 \frac{\partial f_1}{\partial x} \right)_{0^-}, \quad (20)$$

where  $0^+$  and  $0^-$  indicate the positions immediately downstream and upstream of the shock. The quantities  $D \partial f / \partial x$  can be easily computed deriving  $f$  with respect to  $x$  from Eq. (18). We get:

$$\left( D_2 \frac{\partial f_2}{\partial x} \right)_{0^+} = f_0 \frac{u_2}{2} (1 + \sqrt{1 + \Delta_2}) + \int_0^\infty Q_2 e^{-\lambda_2 + x'} dx' \quad (21)$$

and

$$\left( D_1 \frac{\partial f_1}{\partial x} \right)_{0^-} = f_0 \frac{u_1}{2} (1 - \sqrt{1 + \Delta_1}) - \int_{-\infty}^0 Q_1 e^{\lambda_1 - x'} dx'. \quad (22)$$

After a little algebra, the solution of Eq. (20) can be expressed in the following form:

$$f_0(p) = s p^{-s} \int_{p_{\text{inj}}}^p \frac{dp'}{p'} p'^s \frac{G(p')}{u_1} \exp \left\{ -s \int_{p'}^p \frac{dp''}{p''} h(p'') \right\}, \quad (23)$$

where the usual definition of the power law index is  $s = 3u_1/(u_1 - u_2)$ . The injection term  $G$  is the sum of the upstream and downstream contributions,

$$G(p) = \int_{-\infty}^0 Q_1 e^{\lambda_1 - x'} dx' + \int_0^\infty Q_2 e^{-\lambda_2 + x'} dx' \quad (24)$$

while the function  $h$  in the exponential is:

$$h(p) = \frac{1}{2} (\sqrt{1 + \Delta_1(p)} - 1) + \frac{1}{2r} (\sqrt{1 + \Delta_2(p)} - 1). \quad (25)$$

The solution in Eq. (23) shows the typical power law behavior  $\propto p^{-s}$  in the region of momentum where neither injection nor ionization are important, in fact when  $\Delta(p) \ll 1$  then  $h(p)$  vanishes. On the other hand when the ionization length becomes comparable with the diffusion length, i.e.  $\Delta(p) \simeq 1$ , the function  $h(p)$  produces an exponential cutoff in the distribution function.

Now that we got the formal solution we can show some results. Let us start considering the acceleration of He. We

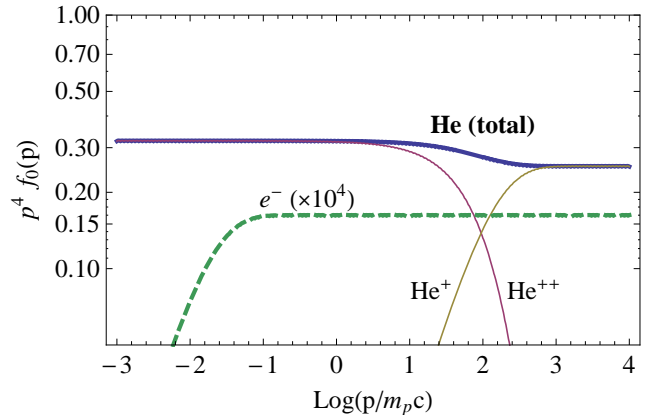


**Figure 5.** Distribution function of Helium at the shock position,  $f_{\text{He},0}(p)$ . The thin solid lines represent the distributions of  $\text{He}^+$  and  $\text{He}^{++}$ , while the thick line is the sum of both the contributions. The dotted lines represent the distribution of electrons (multiplied by  $10^4$ ) ejected in the process  $\text{He}^+ \rightarrow \text{He}^{++} + e^-$ , and subsequently accelerated.

assume that the initial ionization state at the moment of injection is  $\text{He}^+$ . The distribution function  $f_{\text{He}^+}$  is computed with the procedure described above, using the injection term in Eq. (16). We fix  $p_{\text{inj}} = 10^{-3} m_p c$  and the shock velocity equal to 3000 km/s. The photo-ionization time can be an arbitrary function of  $p$ . We use the approximate expression given in Eq. (5). Eqs. (18) and (23) can be integrated numerically. Once  $f_{\text{He}^+}$  is known, we can compute  $f_{\text{He}^{++}}$  using the injection term in Eq. (17), i.e. with  $Q_{\text{He}^{++}} = f_{\text{He}^+} / \tau_{\text{He}^+}$ . The resulting distributions are plotted in Fig. 5 with thin solid lines. We note that  $f_{\text{He}^+} \propto p^{-4}$  up to  $p \simeq 10 m_p c$ ; above such value the distribution of  $\text{He}^+$  drops exponentially while the distribution of  $\text{He}^{++}$  starts rising. It is worth noting that the total distribution (plotted with thick solid line) is slightly steeper than  $p^{-4}$  in the transition region. This effect is due to the different probability which  $\text{He}^+$  and  $\text{He}^{++}$  have to return at the shock once they are downstream. In fact an ion with charge  $Z$  located at the position  $x$  in the downstream has a probability to return at the shock  $\propto e^{-u_2 x/D(Z)}$ ; after the ionization the charge becomes  $Z+1$  and the return probability is reduced by a factor  $e^{-(Z+1)/Z}$ . This translates into a net loss of particles from downstream. This effect of losses is more pronounced when considering heavier elements. In Fig. 6 we show the case of carbon atoms which start the acceleration as singly ionized. The distribution functions of all ionized states are plotted with thin solid lines, from  $\text{C}^+$  up to  $\text{C}^{6+}$ . In the energy region where ionization occurs,  $1.5 < \gamma < 4.5$ , the slope of the total distribution function is  $s \sim 4.1$ .

## 4.2 Spectrum of electrons

Now that we know how to compute the distribution function of ions, the solution for the electron distribution is straightforward. We have to solve the same transport equation (15) writing down the right expression for the electron injection,  $Q_e$ , and dropping the term due to ionization. In the present calculation we neglect energy losses.

Let us consider a single specie  $N$ . From each photo-

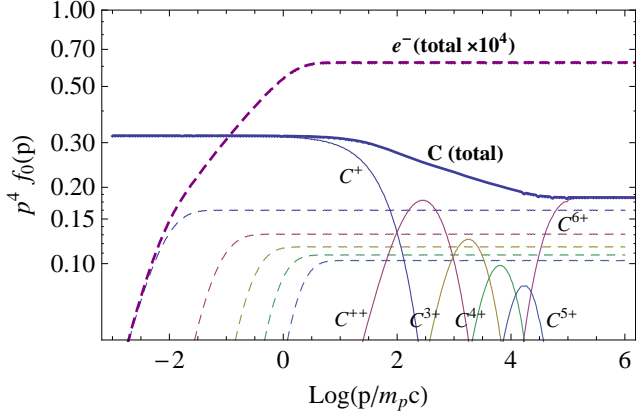


**Figure 6.** Distribution function of Carbon in all the ionization state from  $C^+$  up to  $C^{6+}$ . The thick solid line is the sum of all contributions. The spectra of electrons ejected from each ionization process are plotted with thin dashed lines, while the thick dashed line represent the total sum ( $\times 10^4$ ).

ionization process of the type  $N^Z \rightarrow N^{Z+1} + e^-$ , we have the following contribution to the electron injection:

$$Q_e^{N,Z}(x,p) = \int_p^\infty dp' c \frac{f_N^z(x,p')}{\tau_N^z(p')} \delta^{(3)}(p - \xi_N p') \\ = \xi_N^{-3} \frac{f_{N,1}^z(x,p/\xi_N)}{\tau_N^z(p/\xi_N)} \quad (26)$$

The  $\delta$ -Dirac function in momentum is present because electrons are ejected with the same Lorentz factor of the parent ions, as we discuss in §2. Hence the electron momentum is  $p_e = p_N m_e / m_N \equiv p_N \xi_N$ . Following the procedure used in the previous section, we can write the distribution function for electrons at the shock position as follows:

$$f_{e,0}^{N,Z}(p) = s p^{-s} \xi_N^{s-3} \int_{p_{inj}}^{p/\xi_N} \frac{dy}{y} y^s \frac{G_e^{N,z}(y)}{u_1}. \quad (27)$$

Equation (27) is similar to Eq. (23) with the exception of the multiplying factor  $\xi_N^{s-3}$  and for the absence of the exponential cutoff. We note that the contribution to electron injection from the downstream is negligible with respect to the upstream. This occurs because electrons produced in the downstream have a negligible probability to come back to the shock. The return probability for one electron stripped downstream at a position  $x$  is a factor  $e^{-m_N/Z_N m_e}$  smaller than the return probability of the parent ion. Hence in the injection term we consider only the contribution from upstream, which reads:

$$G_e^{N,Z}(p) = \int_{-\infty}^0 Q_e^{N,Z}(x',p) dx'. \quad (28)$$

In Figs. 5 and 6, besides the distribution of ions, we plot also the distributions of the electrons due to each single ionization step, multiplied by  $10^4$  (dashed lines). Comparing Eqs. (23) and (27) we see that the ratio between electron and ion distribution functions is:

$$K_{eN} \equiv f_{e,0}^{N,Z}(p) / f_{N,0}^z(p) = \xi_N I_{N,Z}(p). \quad (29)$$

The function  $I_{N,Z}(p)$  represents the ratio between the injection integrals in Eqs. (23) and (27). It can be computed

numerically and in the asymptotic limit  $p \gg p^*$  (where  $p^*$  is such that  $\Delta(p^*) = 1$ ) it is  $I_{N,Z} \sim Z/(2Z-1)$ . This result is not surprising: it reflects the fact that for each ionization event electrons can be injected only if they are released upstream hence their number is roughly 1/2 of the injected ions.

Now we are interested in the total number of accelerated electrons that can be produced via the ionization process. In the literature the number of electrons is usually compared with that of accelerated protons: DSA operates in the same way for both kinds of particles, hence a proportionality relation between their distribution functions is usually assumed, i.e.  $f_e(p) = K_{ep} f_p(p)$ . From the observational point of view, the value of  $K_{ep}$  in the source strongly depends on the assumption for the magnetic field strength in the region where electrons radiate and, in the context of the DSA theory, it can be determined for those SNRs where both non thermal X-ray and TeV radiation are observed. Two possible scenarios have been proposed. In the first one electrons produce both the X-ray and the TeV components via the synchrotron emission and the inverse Compton effect, respectively; this scenario requires a downstream magnetic field around  $20 \mu\text{G}$ , and  $K_{ep} \sim 10^{-2} - 10^{-3}$ . The second scenario assumes that the number of accelerated protons is large enough to explain the TeV emission as due to the decay of neutral pions produced in hadronic collisions. In this case the DSA requires a magnetic field strength of few hundreds  $\mu\text{G}$  and  $K_{ep} \sim 10^{-4} - 10^{-5}$ . Such a large magnetic field is consistently predicted by the theory as a result of the magnetic amplification mechanisms which operate when a strong CR current is present. In Table 2 we report some examples of young SNRs where the nonlinear theory of acceleration has been applied to fit the multi-wavelength spectrum. The fourth and fifth columns report the estimated value of the downstream magnetic field strength and the corresponding electron/proton ratio.

In order to give an approximated estimate for  $K_{ep}$  we need to multiply Eq. (29) by the total number of ejected electrons, i.e.  $(Z_N - Z_{N,0})$ , and sum over all atomic species present in the accelerator, i.e.  $K_{ep} \simeq \sum_N K_{Np} (Z_N - Z_{N,\text{eff}}) K_{eN}$ .  $K_{Np}$  are the abundances of ions measured at the source in the range of energy where the ionization occurs. Even if the values of  $K_{Np}$  are widely unknown, we can estimate them using the abundances measured at Earth and adding a correction factor to compensate for propagation effects in the Galaxy, namely the fact that particles with different  $Z$  diffuse in a different way. The diffusion time in the Galaxy is usually assumed to be  $\tau_{\text{diff}} \propto (p/Z)^{-\delta}$ , with  $\delta \approx 0.3 - 0.6$  (see Blasi (2007) for a review on recent CR experiments). If  $K_{Np,0}$  is the ion/proton ratio measured at Earth, than the same quantity measured at the source is  $K_{Np} = K_{Np,0} Z_N^{-\delta}$ . Hence the final expression for the electron/proton ratio at the source is:

$$K_{ep} = \sum_N K_{Np,0} Z_N^{-\delta} (Z_N - Z_{N,0}) \frac{Z_N}{2Z_N - 1} \left( \frac{m_e}{m_N} \right)^{s-3}. \quad (30)$$

In Fig. 7 we report the value of  $K_{ep}$  computed according to Eq. (30) as a function of the spectral slope  $s$  and for  $\delta = 0.3$  and  $0.6$ . For  $K_{Np,0}$  we use the abundances of nuclei in the CR spectrum measured at 1 TeV (Wiebel-Sooth et al. 1998). Moreover we determine the initial charge of different species,  $Z_{N,0}$ , adopting the thermal equilibrium in a plasma

SNR	Age (yr)	$d(\text{kpc})$	$B_2(\mu\text{G})$	$K_{ep}/10^{-4}$	ref.
Kepler	400	3.4–7.0	440–500	0.7–2.8	( <i>a</i> )
Tycho	430	3.1–4.5	368–420	4.2–15	( <i>b</i> )
SN 1006	1000	1.8	90	1.3	( <i>c</i> )
"	"	2.2	120	4.1	( <i>d</i> )
G347.3-0.5	1600(?)	1.0	100	0.6	( <i>e</i> )
"	"	1.0	130	1.0	( <i>f</i> )

**Table 2.** Estimated value for the magnetic field and  $K_{ep}$  for some young supernova remnants. Results are from: (*a*) Berezhko et al. (2006), (*b*) Völk et al. (2008), (*c*) Morlino et al. (2010), (*d*) Berezhko et al. (2009), (*e*) Morlino et al. (2009), (*f*) Berezhko & Völk (2006).

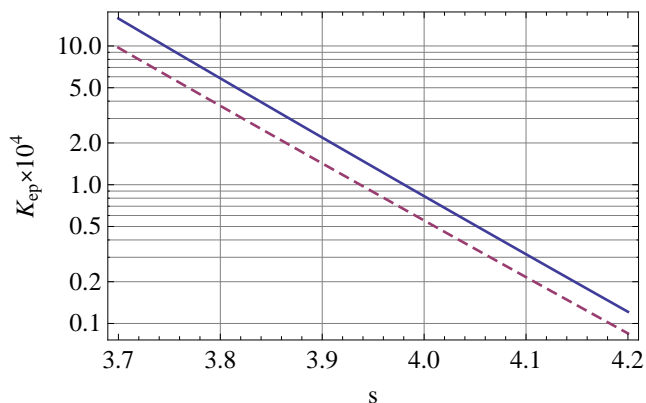


**Figure 7.** Value of  $K_{ep}$  computed from Eq. (30) as a function of the slope  $s$  and for  $\delta = 0.6$  (solid line) and  $\delta = 0.3$  (dashed line).

with a temperature  $T \sim 10^5$ . Remarkably using the slope predicted by linear theory for strong shock,  $s = 4$ , we have  $K_{ep} \sim 10^{-4}$ : this number gives the right order of magnitude required to explain the values of  $K_{ep}$  reported in Table 2. We stress here that in order to provide a better estimate of  $K_{ep}$  for a specific SNR we should know the local chemical composition and have a realistic model for the injection of heavy elements into the DSA, which can provide the right value of  $Z_{N,0}$ .

Equation (30) has been obtained using the test particle approach. A better estimate requires the use of nonlinear theory which is, indeed, much more complicated to develop. Nevertheless it is easy to realize that the main effect that nonlinearity can produce on  $K_{ep}$  is due to the different prediction of the slope  $s$ . In fact, while the test particle approach gives the universal slope  $s = 4$ , the nonlinear theory predict concave spectra with  $s = s(p)$ . The basic formulation of the nonlinear theory usually leads to  $s > 4$  for momenta lower than  $\sim 10Z^{-1}$  GeV/c and  $s < 4$  for larger momenta (Amato & Blasi 2005). As discussed in §2, ionization typically occurs for  $\gamma \gtrsim 10$ , where the slope is  $s < 4$ . Hence we can conclude that the nonlinear effects tend to increase the value of  $K_{ep}$ . For instance, from Fig. 7 we see that for  $s = 3.7$ ,  $K_{ep}$  rises up to  $\sim 10^{-3}$ .

It is worth noting that nonlinear effects can also result in the opposite situation with  $K_{ep} < 10^{-4}$ , as we will show below. A key ingredient of the DSA is the speed of the magnetic turbulence which is responsible for particles scattering. The speed of the scattering centers contributes to the deter-

mination of the effective compression ratio felt by particles which, in turns, determines the spectral slope. The typical speed of the turbulence is of the order of Alfvén speed which, when is computed in the background magnetic field, is of the order of few tens km/s and it is negligible with respect to the shock speed. On the other hand if one assume that turbulence moves with the Alfvén speed computed in the amplified magnetic field, as shown by Caprioli et al. (2010), it cannot be neglected and the resulting slope can be  $> 4$ . If this happens the value of  $K_{ep}$  drops and the number of electrons produced via ionization is maybe insufficient in order to explain the synchrotron emission.

A final comment concerns the mechanism of electrons injection in core-collapse SNRs. The value of  $K_{ep}$  shown in Fig. 7 has been computed using the ionization level of chemical elements in a plasma with  $T \sim 10^5$ . We recall that the type I/a SNRs expand in the warm ISM, where the typical temperature is around  $10^4$  K hence we expect the injection of electrons to be relevant. On the other hand core-collapse SNRs expands into a diluted bubble whose temperature reach  $10^6$  K (Higdon & Lingenfelter 2005), hence the degree of ionization of atoms is higher and the number of electrons available for the injection is smaller (see e.g. Porquet et al. (2001)). Using  $T = 10^6$  we estimate that  $K_{ep}$  is a factor  $\sim 4$  smaller than the values shown in Fig. 7. On the other hand in those bubbles the metallicity is estimated to be greater than the ISM mean value (Higdon & Lingenfelter 2005). Hence, even for core-collapse SNRs the electron injection through ionization could play a relevant role.

## 5 DISCUSSION AND CONCLUSIONS

In this work we include for the first time the ionization process of heavy ions in the theory of DSA at SNR shocks. We showed that, for the typical environments where SNRs propagate, the photo-ionization due to the ISRF dominates on the collisional ionization and produces two important effects: 1) the reduction of the maximum energy achieved by ions and 2) the production of a relativistic population of electrons.

(1) The first effect is especially important for the interpretation of the knee structure in the all particle spectrum of CRs. The change of slope on the two sides of the knee is generally interpreted as due to the superposition of spectra of chemicals with different nuclear charges combined with their abundances and convolved with the rigidity dependent diffusion in the Galaxy. An important requirement for a good fit to the knee is that the cutoff energy of each specie, from hydrogen up to iron, should be proportional to the nuclear charge,  $Z_N$ .

It is generally assumed that DSA can accelerate ions up to a maximum energy proportional to  $Z_N$ . This assumption is valid only if the ionization time needed to strip all electrons from atomic orbitals,  $\tau_{\text{ion}}^{\text{tot}}$ , is much shorter than the acceleration time. We assume that the maximum possible acceleration time is equal to the Sedov-Taylor time,  $t_{ST}$ , corresponding to the end of the free expansion phase. Using a simple steady-state approach we showed that, especially for very massive ions,  $\tau_{\text{ion}}^{\text{tot}}$  can be comparable to or even larger than  $t_{ST}$ , depending on the type of the remnant and on its location in the Galaxy. In fact the ISRF

responsible for the photo-ionization decreases for increasing distance from the Galactic Center. We analyze two different cases which are representative of a type I/a and a core-collapse SNRs. Our main results are the following. SNRs of type I/a are generally unable to accelerate ions according to  $E_{\max,N} \propto Z_N$  because  $t_{ST}$  does not exceed the typical value of 500 yr. The only exception are the remnants located in the Galactic bulge where the photon field is strong enough to reduce the photo-ionization time to a value much shorter than  $t_{ST}$ . The situation for core-collapse SNRs is different because their typical Sedov time is  $\gtrsim 2000$  yr hence the ionization time for chemicals up to iron can be neglected and the maximum energy is indeed proportional to the nuclear charge, with the exception of those remnant located very far away from the Galactic Center where the ISRF is very low.

Previous conclusions are based on the assumption that during the free expansion phase both the magnetic field and the shock velocity remain constant. This is indeed a poor approximation. In fact during the free expansion phase the shock speed can vary by a factor of few (depending on the velocity profile of the ejecta and on the density profile of the external medium). Now for DSA the acceleration rate is proportional to  $u_{sh}^2 \delta B(u_{sh})$ , where  $\delta B(u_{sh})$  is the turbulent magnetic field generated by the CR induced instabilities (resonant or non-resonant), which is an increasing function of the shock velocity. Hence the acceleration rate can significantly change during the free expansion phase even if  $u_{sh}$  varies only by a factor of few. Always in the framework of steady-state approximation, we develop a simple toy model able to include the magnetic field amplification and the time evolution of the remnant. Using this toy model we showed that the magnetic amplification and time evolution can significantly reduce the acceleration time with respect to  $t_{ST}$  and, as a consequence, the maximum energy achieved by heavy ions becomes smaller than the previous estimate: the relation  $E_{\max,N} \propto Z_N$  can be achieved up to iron nuclei only by SNRs with a Sedov time  $\gg 10^3$  yr which means that the mass ejecta should be  $\gg 1 M_\odot$ .

Clearly the same mechanism also applies to ions heavier than Fe. Their maximum energy cannot be much larger than that achieved by Fe itself unless the acceleration occurs in very massive SNRs. Hence the ionization mechanism put severe limitation to the possibility that ultra heavier ions can contribute to the CR spectrum in the transition region between Galactic and extragalactic component.

(2) The second effect concerning the production of relativistic electrons was already put forward in Morlino (2009). The ionization mechanism provides a source for the injection of relativistic electrons into the DSA mechanism. We investigate the possibility that those electrons can be responsible for the synchrotron radiation observed from young SNRs. In order to estimate the total number of injected electrons we use a semi-analytical technique to solve the steady-state transport equation which describe the electron distribution function in the shock region. Summing the contributions coming from the ionization of all chemicals we showed that the ratio between accelerated electrons and protons is  $K_{ep} \sim 10^{-4}$ . This value is especially appealing because corresponds to the right order of magnitude required in order to explain the synchrotron emission if the magnetic field is amplified up to few hundreds  $\mu\text{G}$ . Interestingly such magnetic field amplification is consistently predicted by non linear ac-

celeration theory as a consequence of the back reaction of accelerated particles onto the shock dynamics.

Several effects can modify our prediction for the number of electrons. The estimate  $K_{ep} \sim 10^{-4}$  is obtained using test particle approximation and adopting the abundances of CR spectrum observed at the Earth corrected for the effect of propagation in the Galaxy. Even if we did not develop a fully nonlinear approach, we showed how nonlinear effects can substantially modify the electron/proton ratio. Indeed the value of  $K_{ep}$  strongly depends on the spectral slope as one can see from Eq. (30). Nonlinear DSA usually predicts steeper spectra than the test particle result,  $s = 4$ , and this translates into an enhancement of  $K_{ep}$ . On the other hand also the opposite situation can be realized. Indeed some authors pointed out that, if the magnetic field amplification occurs, the velocity of the magnetic turbulence with respect to the plasma can be much larger than the Alfvén speed corresponding to the background magnetic field. If this occurs the spectral slope of the accelerated particles be appreciably softer than 4 and the electron/proton ratio would drop to a value which is insufficient to explain the observed synchrotron radiation.

In order to get a correct determination of  $K_{ep}$  for a single SNR, other effects should be taken into account: *a)* the chemical composition of the environment where the SNR expands, *b)* the initial ionization state of each chemicals and *c)* a realistic model for the ions injection. A further complication directly related to the previous points is the fact that many heavy elements are condensed in solid dust grains both in the ISM as well as in the stellar wind. It has been pointed out that the injection of refractory elements into the DSA can be dominated by the sputtering of these dust grains rather than by the injection of single atoms from the thermal bath (Ellison, Drury & Meyer 1997). In this picture a correct computation of the number of injected ions and their initial ionization state is very challenging.

As a finally remark we want to stress that the electron/proton ratio in a single source, what we call  $K_{ep}$ , is different from the same ratio measured from the CR spectrum at Earth, which is  $5 \cdot 10^{-3}$  at 1 TeV (Blasi 2007). Sometimes these quantities are assumed to be the same. Conversely they could be different because the latter is the sum of the contribution coming from all sources integrated during the source age, and also reflect transport to Earth and losses in transport. Especially relevant is the fact that other sources like pulsar wind nebulae can significantly contribute to the electron flux measured at Earth, but not to the proton flux. Moreover the value of  $K_{ep}$  in a single source can vary during the source age. Different mechanisms of electron injection, other than the ionization, can be relevant in different phases of the remnant.

## ACKNOWLEDGMENTS

I am grateful to P. Blasi, E. Amato and D. Caprioli for useful and continuous discussions and exciting collaboration. I also wish to thank the *Kavli Institute for Theoretical Physics* in Santa Barbara where part of this work was done during the program *Particle Acceleration in Astrophysical Plasmas*, July 26-October 3, 2009. This research was founded through the contract ASI-INAF I/088/06/0 (grant TH-037).

REFERENCES

- Allen, C. W., *Astrophysical quantities*, 3<sup>rd</sup> ed., The Athlone Press LTD, London, 1973
- Amano, T., Hoshino, M., 2009, ApJ, 690, 244
- Amato, E., Blasi, P., 2005, MNRAS, 364, L76
- Antoni, T. et al. (KASCADE collaboration), 2005, APh, 24, 1
- Bell A. R., 2004, MNRAS, 353, 550
- Berezhko, E. G., Völk, H. J., 2006, A&A, 451, 981
- Berezhko, E. G., Ksenofontov, L. T., Völk, H. J., 2006, A&A, 440, 500
- Berezhko, E. G., Ksenofontov, L. T., Völk, H. J., 2009, A&A, 505, 169
- Bethe, H., 1930, 1930, Ann. Phys., 5, 325
- Blasi, P., 2007, rapporteur Paper - OG1 session of the 30th ICRC, Merida, Mexico. arXiv:0801.4534
- Blasi P., 2002, APh, 16, 429
- Blasi, P., Amato, E., Caprioli, D., 2007, MNRAS, 375, 1471
- Caprioli, D., Blasi, P., Amato, 2011, APh, 34, 447
- Caprioli, D., Amato, E., Blasi, P., 2010, APh, 33, 307
- Caprioli, D., Blasi, P., Amato, E., Vietri, M., 2009, MNRAS, 395, 895
- Chevalier, R. A., Kirshner, R. P., Raymond, J. C., 1980, ApJ, 235, 186
- Ellison, D. C., Drury, L. O'C., Meyer, J. P., 1997, ApJ, 487, 197
- Galeev, A. A., 1984, AdSpR, 4, 255
- Heitler, W., *The Quantum Theory of Radiation*, Oxford University Press, London, 1954
- Heng, K., 2009, PASA, 27, 23
- Higdon, J. C. & Lingenfelter, R. E., 2005, ApJ, 628, 738
- Hörandel, J. R., 2003, APh., 19, 193
- Inokuti, M., 1971, Rev. Mod. Phys., 43, 297
- Kim, Y. K, Santos, J. P., Parente, F., 2000, Phys. Rev. A, 62, 052710
- Levinson, A., 1992, ApJ, 401, 73
- Levinson, A., 1996, MNRAS, 278, 1018
- Morlino G., 2009, PRL, 103, 121102
- Morlino, G., Amato, E., Blasi, P., 2009, MNRAS, 392, 240
- Morlino, G., Amato, E., Blasi, P., Caprioli, D., 2010, MNRAS, 405L, 21
- Porquet, D., Arnaud, M. & Decourchelle, A., 2001, A&A, 373, 1110
- Porter, T. A. and Strong, A. W., 2005, proc. 29th ICRC 4, 77
- Riquelme, M. A., Spitkovsky, A., 2010, preprint arXiv:1009.3319v1
- Sollerman, J., Ghavamian, P., Lundqvist, P., Smith, R. C., 2003, A&A, 407, 249
- Truelove, J. K. & McKee, C. F., 1999, ApJS, 120, 299
- Völk, H. J., Berezhko, E. G., Ksenofontov, L. T., 2008, A&A, 483, 529
- Wiebel-Sooth, B., Biermann, P. L., Meyer, H., 1998, A&A, 330, 389